Citation: BoneKEy Reports **4**, Article number: 645 (2015) | doi:10.1038/bonekey.2015.12

www.nature.com/bonekey

ORIGINAL ARTICLE

Exercise prevents β-aminopropionitrile-induced morphological changes to type I collagen in murine bone

Max A Hammond[1] and Joseph M Wallace[1,2,3]

[1]Weldon School of Biomedical Engineering, Purdue University, West Lafayette, Indianapolis, IN, USA. [2]Department of Biomedical Engineering, Indiana University-Purdue University at Indianapolis, Indianapolis, IN, USA. [3]Department of Orthopaedic Surgery, Indiana University School of Medicine, Indianapolis, IN, USA.

This study evaluated the effects of reduced enzymatic crosslinking, exercise and the ability of exercise to prevent the deleterious impact of reduced crosslinking on collagen D-spacing. Eight-week-old female mice were divided into four weight-matched groups receiving daily injections of either phosphate-buffered saline (PBS) or 300 mg kg^{-1} β-aminopropionitrile (BAPN) while undergoing normal cage activity (Sed) or 30 min per day of treadmill exercise (Ex) for 21 consecutive days. BAPN caused a downward shift in the D-spacing distribution in Sed BAPN compared with Sed PBS ($P < 0.001$) but not in Ex BAPN ($P = 0.429$), indicating that exercise can prevent changes in collagen morphology caused by BAPN. Exercise had no effect on D-spacing in PBS control mice ($P = 0.726$), which suggests that exercise-induced increases in lysyl oxidase may be a possible mechanism for preventing BAPN-induced changes in D-spacing. The D-spacing changes were accompanied by an increase in mineral crystallinity/maturity due to the main effect of BAPN ($P = 0.016$). However, no changes in nanoindentation, reference point indentation or other Raman spectroscopy parameters were observed. The ability of exercise to rescue BAPN-driven changes in collagen morphology necessitates further research into the use of mechanical stimulation as a preventative therapy for collagen-based diseases.

BoneKEy Reports **4**, Article number: 645 (2015) | doi:10.1038/bonekey.2015.12

Introduction

Bone is an exquisite material with a structural hierarchy spanning several orders of magnitude in length scale.[1] At the nanoscale, bone is a composite material of type I collagen and carbonated hydroxyapatite, but it is not well understood how changes occurring at this scale (for example alterations in individual collagen molecules or fibrils) influence the mechanical properties at higher length scales. Structurally, collagen is composed of tropocollagen molecules that aggregate in a parallel staggered array to form a collagen fibril with a characteristic period of gaps and overlaps known as the D-period.[2] This structural feature of collagen is functionally important as collagen forms the template for mineralization in bone, and evidence suggests that mineralization begins in the gap regions.[3] This collagen-reinforced composite adds tensile strength to bone[4] and provides toughness as fibrils are allowed to slip past one another under applied loading.[5]

In bone an additional toughening mechanism is mediated by enzymatic covalent crosslinks, which both stabilize collagen fibrils and may sacrificially rupture during loading, protecting the collagen backbone and mineral from damage.[6] Enzymatic crosslinks occur between adjacent lysine or hydroxylysine residues that have been deaminated by the enzyme lysyl oxidase (LOX) resulting in a reactive aldehyde.[7] Osteolathyrism, a bone disease characterized by bone pain and skeletal deformities,[8] is caused by a reduction in the quantity of enzymatically crosslinked collagen due to dietary intake of toxins (lathyrogens) present in seeds from the *Lathyrus* genus, which block crosslink synthesis.[9] The sweet pea (*Lathyrus odoratus*) contains β-aminopropionitrile (BAPN),[10] which irreversibly binds to the LOX active site,[11] and is a commonly used lathyrogen to experimentally replicate osteolathyrism.[12–15] Understanding the implications of reduced enzymatic crosslinking is important because crosslinks are reduced with aging and other diseases such as diabetes and osteoporosis.[16] Therefore, treatment with BAPN can serve as a model of osteolathyrism and further our understanding of how nanoscale changes in collagen impact bone strength and fracture resistance.

Correspondence: Professor JM Wallace, Department of Biomedical Engineering, Indiana University-Purdue University at Indianapolis, 723 W Michigan Street SL220D, Indianapolis, IN 46202, USA.
E-mail: jmwalla@iupui.edu

Received 1 October 2014; accepted 27 January 2015; published online 11 March 2015

Exercise is beneficial to bone because increased mechanical stimulation from exercise can lead to increased mass and optimized structure as bone adapts.[17] The adaptive changes in mass and structure can allow bone to withstand higher loads. However, the mechanical integrity of bone also depends on the material properties of the underlying tissue. Exercise-induced increases in postyield displacement strongly suggest that tissue quality is favorably altered by exercise.[18] Postyield displacement is generally thought to be driven by the organic phase of bone,[6,19] which may indicate that exercise improves collagen quality given that bone's organic matrix is 90% type I collagen. If true, exercise may be a potent noninvasive treatment for collagen-based disease.

The aim of this work was to investigate the effects of BAPN treatment and exercise on collagen nanoscale morphology. Preliminary mechanical and compositional characterizations of these effects were also analyzed. It was hypothesized that decreased crosslinking associated with BAPN treatment would change collagen morphology and detrimentally impact bone material properties. Exercise during treatment would prevent these changes and maintain collagen morphology near control levels.

Results

Animals

One mouse was excluded from the exercise regimen (Ex) phosphate-buffered saline (PBS) group because it was not able to complete the exercise protocol. Throughout the study, group weights were statistically indistinguishable from one another.

Atomic force microscopy

After pooling fibril measurements for each sample, the mean and s.d. for normal cage activity (Sed) PBS, Sed BAPN, Ex PBS and Ex BAPN were 65.8 ± 0.5, 65.4 ± 0.5, 65.7 ± 1.0 and 66.0 ± 0.5 nm, respectively. There were no significant effects or interactions for mean D-spacing. However, the D-spacing distribution of Sed BAPN was significantly shifted to lower values (**Figure 1a**, $P < 0.001$). The distributions of Sed PBS and Ex PBS were not significantly different (**Figure 1b**, $P = 0.429$). Although exercise alone did not affect the D-spacing distribution, exercise in BAPN-treated animals restored the distribution to a state that was indistinguishable from Sed PBS (**Figure 1c**, $P = 0.726$).

Nanoindentation

Although Ex BAPN had a qualitatively greater reduced modulus (14.174 ± 2.303 GPa) compared with Sed PBS, Ex PBS and Sed BAPN (12.857 ± 1.736, 11.936 ± 3.731 and 11.386 ± 2.531 GPa, respectively), there were no significant main effects or interactions using nanoindentation. The same nonsignificant trend was observed for hardness as Ex BAPN was harder than Sed PBS, Ex PBS and Ex BAPN (0.739 ± 0.187, 0.632 ± 0.123, 0.581 ± 0.229 and 0.548 ± 0.159 GPa, respectively).

Raman spectroscopy

Mineral-to-matrix ratios were not significantly altered by BAPN treatment or exercise, and no significant interaction effect was observed (**Table 1**). No significant differences in type B carbonate substitution were found for either main effects or their interaction. However, mineral crystallinity/maturity was significantly altered by BAPN treatment ($P = 0.016$). Sed BAPN (0.0537 ± 0.0004) and Ex BAPN (0.0540 ± 0.0004) had crystallinity measures greater than both Sed PBS (0.0535 ± 0.0003) and Ex PBS (0.0532 ± 0.0004), contributing to the significance of the effect of BAPN. The interaction between BAPN and exercise was not significant for crystallinity/maturity.

Reference point indentation

First cycle creep indentation distance (CID 1st), indentation distance increase (IDI) and average creep indentation distance (CID Avg) were non-normal, but after implementing reciprocal transformations, normality for all three parameters was restored. Variance heterogeneity for 1st cycle unloading slope (US 1st) was corrected with a reciprocal transformation. As seen in **Table 2**, reference point indentation (RPI) did not reveal any differences for either BAPN treatment, exercise or their interaction.

Discussion

This study indicates that as BAPN binds lysyl oxidase, enzymatic crosslinks within collagen fibrils are reduced,[15] which alters fibril morphology as shown by the downward shift in the population of fibril D-spacing (**Figure 1a**). A similar downward shift in D-spacing distribution was observed in a murine model of osteogenesis imperfecta.[20] In a rat model of type 2 diabetes mellitus, increased non-enyzmatic crosslinking tended to shift the D-spacing distribution up in bone and tendon, suggesting that greater overall crosslinking (whether enzymatic or non-enzymatic) is associated with increased D-spacing distributions.[21,22] The downward shift reported here was rectified to PBS control levels when exercise was introduced in BAPN mice (**Figure 1c**). However, exercise alone had no effect on the distribution in PBS control mice (**Figure 1b**), indicating that a direct mechanical effect of exercise was not responsible for the shift. A possible explanation for exercise's ability to rescue the D-spacing distribution while causing no independent effect is an exercise-induced increase in LOX production. Mechanical loading is known to increase LOX expression in preparation for an anabolic modeling response.[23,24] Because LOX acts only on lysine and hydroxylysine residues at specific sites in collagen α-helices,[7] increased LOX with exercise in PBS control mice would not have an effect on D-spacing because there is already sufficient functional LOX to catalyze these residues. In the BAPN groups, there is a reduction in the amount of functional LOX. However, the exercise-induced increase in LOX in BAPN mice could restore the overall functional amount of LOX to near-normal levels, which would explain the normal D-spacing distribution observed here.

Crystallinity/maturity in the distal tibia increased as a response of the main effect of BAPN [from a two-way analysis of variance (ANOVA); **Table 1**]. Given the intimate relationship between mineral and collagen, it is not surprising to observe changes to the mineral phase of bone given the clear morphological difference in collagen demonstrated with atomic force microscopy (AFM) in the Sed BAPN group. However, exercise prevents the morphological change from BAPN, suggesting that separate mechanisms may be driving the increased crystallinity observed in Sed BAPN and Ex BAPN groups. Measures of crystallinity using Raman are sensitive to changes in size, perfection, carbonate substitutions and heterogeneity.[25,26] Therefore, it is reasonable to potentially

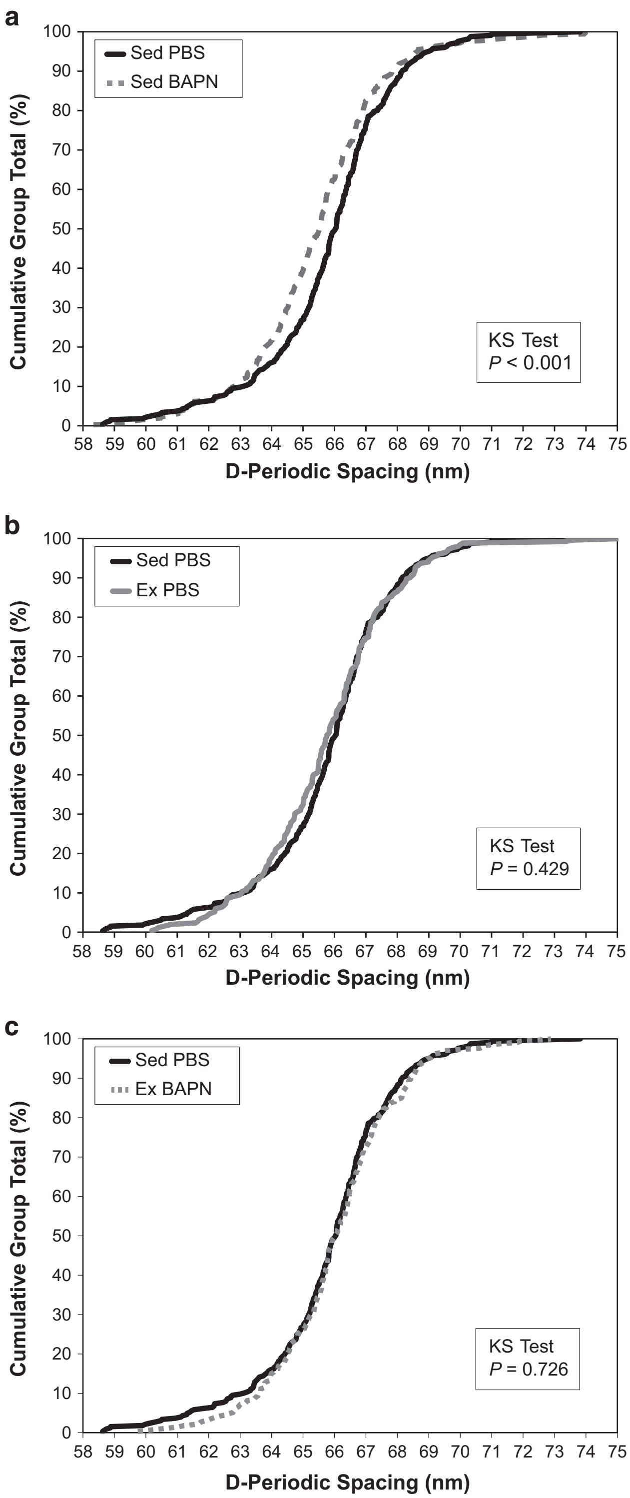

Figure 1 Collagen D-spacing distributions. (**a**) BAPN significantly altered the D-spacing distribution in sedentary mice by shifting D-spacing downward. Sed BAPN, $n = 355$ fibrils. Sed PBS, $n = 326$ fibrils. (**b**) Exercise does not alter D-spacing in PBS control mice. Ex PBS, $n = 252$ fibrils. (**c**) BAPN administration concurrent with exercise does not have an effect on D-spacing vs PBS control mice. Ex BAPN, $n = 332$ fibrils.

observe separate mechanisms at work. In Sed BAPN, increased crystal perfection may occur because of the removal of steric interference from crosslinks that are not present in the region. Whereas in Ex BAPN, the increased crystallinity may be driven by qualitative decreases in the amount of carbonate substitution, which is the lowest among all groups in Ex BAPN (**Table 1**). Although the specific mechanisms responsible are not clear, changes in crystallinity because of BAPN treatment is an interesting finding that warrants further investigation using more direct methods of evaluating changes to the crystalline structure.[27] Another study demonstrated no effects on crystallinity/maturity with BAPN treatment,[13] but these conflicting data may be due to differences in dose ($\sim$780 vs 300 mg kg^{-1}), method of delivery (dietary vs subcutaneous injection), animal model (rat vs mouse) and anatomical site (vertebral cross-section vs native surface of femur).

The dosage of BAPN administered in this study is expected to incompletely inhibit LOX. Given a mouse of 18.6 g (grand mean of all groups over entire study), 5.58 mg of BAPN would be administered at a concentration of 218 mM. Assuming a 72 ml kg^{-1} blood volume,[28] the concentration of BAPN in blood would be $\sim$30 mM. Extrapolating from data on the pharmacokinetics of BAPN from intraperitoneal injections in mice[29] and intravenous injections in rabbits,[12] BAPN remains in the serum of mice from the present study at a concentration above the half-maximal inhibitory concentration (IC_{50}) of 25 μM[30,31] for 3.5–10 h after injection before moving to secondary compartments (such as bone) or being cleared. Given this time-scale, the proposed mechanism of restoring D-spacing distribution in bone through exercise-induced increases in LOX is reasonable as a modest increase in LOX would allow for more LOX to be functional for a longer period of time between daily injections.

This study was designed to detect differences in collagen D-spacing distributions with BAPN treatment and exercise. As such, it was underpowered to make strong claims about effects on bone mechanical integrity or chemical composition. Nanoindentation, RPI and Raman spectroscopy are subject to larger biological variation vs collagen D-spacing distributions. An increase in sample size in future studies is necessary to investigate these parameters. However, given the low sample sizes, the observed significant increase in crystallinity caused by BAPN is compelling. Spectroscopic crosslinking ratios were not calculated because of the increased noise in the amide I region associated with Raman rather than Fourier transform infrared spectroscopy, which did not allow underlying peaks to be accurately fit or identified using the recommended second derivative analysis.[32] The purpose of this study was to investigate effects specifically on type I collagen in bone. Because the LOX binding sites are conserved in other fibrillar types of collagen[33,34] and as other tissues besides bone contain type I collagen, BAPN treatment is expected to have effects in other tissue types, but these were not considered here.

BAPN treatment alters the nanoscale morphology of type I collagen fibrils causing a downward shift in the D-spacing distribution. Exercise in the presence of BAPN treatment restores this D-spacing distribution to a level that is indistinguishable from the control state. The implications of the shifts in D-spacing distribution to bone quality are unclear, but the ability of exercise to rescue collagen morphology in this disease state necessitates further research into the mechanical effects associated with BAPN-induced nanostructural changes and their exercise-mediated prevention. Future studies will investigate the molecular mechanisms underlying these changes and their implications to whole bone mechanical integrity and fracture resistance.

Table 1 Raman spectroscopy of distal tibia

	Sed PBS	*Sed BAPN*	*Ex PBS*	*Ex BAPN*
Crystallinity/maturity*	0.0535 ± 0.0003	0.0537 ± 0.0004	0.0532 ± 0.0004	0.0540 ± 0.0004
PO_4^{3-} ν1/amide I	2.58 ± 0.32	2.47 ± 0.13	2.49 ± 0.16	2.80 ± 0.39
CO_3^{2-} ν1/PO_4^{3-} ν1	0.628 ± 0.032	0.657 ± 0.036	0.615 ± 0.082	0.590 ± 0.081
PO_4^{3-} ν1/amide III	3.69 ± 0.44	3.52 ± 0.29	3.64 ± 0.10	3.68 ± 0.56
PO_4^{3-} ν1/CH_2 wag	4.00 ± 0.34	3.71 ± 0.17	3.92 ± 0.28	3.79 ± 0.62

Abbreviations: BAPN, β-aminopropionitrile; Ex, exercise regimen; PBS, phosphate-buffered saline; Sed, normal cage activity. Values presented as mean ± s.d. $n = 4$–5 per group. *$P < 0.05$ effect of BAPN.

Table 2 RPI from distal tibia

	Sed PBS	*Sed BAPN*	*Ex PBS*	*Ex BAPN*
ID 1st (μm)	35.4 ± 3.9	35.0 ± 1.4	40.1 ± 4.8	36.4 ± 4.4
ED 1st (μJ)	30.0 ± 4.3	31.1 ± 2.8	36.0 ± 7.8	32.4 ± 6.8
US 1st (N μm^{-1})	0.240 ± 0.036	0.252 ± 0.035	0.226 ± 0.022	0.246 ± 0.008
CID 1st (μm)	3.62 ± 0.50	3.87 ± 0.49	4.30 ± 1.37	3.86 ± 0.91
IDI (μm)	6.50 ± 0.50	7.50 ± 1.15	7.73 ± 2.72	6.89 ± 2.05
TID (μm)	39.1 ± 3.6	39.5 ± 2.2	44.3 ± 6.1	40.2 ± 5.5
ED Tot (μJ)	73.0 ± 5.5	75.5 ± 4.3	78.5 ± 13.5	72.7 ± 11.6
Avg CID (μm)	1.32 ± 0.17	1.32 ± 0.16	1.37 ± 0.27	1.29 ± 0.16
Avg ED (μJ)	4.4 ± 0.4	4.6 ± 0.6	4.4 ± 0.6	4.2 ± 0.5
Avg US (N μm^{-1})	0.250 ± 0.039	0.259 ± 0.038	0.235 ± 0.020	0.252 ± 0.010

Abbreviations: BAPN, β-aminopropionitrile; Avg CID, average creep indentation distance; CID 1st, first cycle creep indentation distance; ED Avg, average energy dissipation of cycles 3-10; ED Tot, total energy dissipation; ED 1st, 1st cycle energy dissipation; Ex, exercise regimen; ID 1st, 1st cycle indentation distance; IDI, indentation distance increase; PBS, phosphate-buffered saline; RPI, reference point indentation; Sed, normal cage activity; TID, total indentation distance; Avg US, average unloading slope; US 1st, 1st cycle unloading slope. Values presented as mean ± s.d. $n = 4$–5 per group.

Materials and Methods

Animals

Eight-week-old female C57BL/6 mice were separated into four weight-matched groups ($n = 5$ per group) with prior IACUC approval (SC210R). Mice experienced either Sed or Ex previously shown to alter bone structural and tissue-level mechanical properties.[35] All mice had access to food, water and cage activity *ad libitum*. Ex animals ran on a treadmill (Animal Treadmill: Exer 3/6; Columbus Instruments, Columbus, OH, USA) for 30 min per day at 12 m min^{-1} on a 5° incline for 21 consecutive days. The mice received daily 200 μl subcutaneous injections of either PBS or BAPN (300 mg kg^{-1} in PBS). Mice were weighed every other day beginning on day 0 and ending on day 19 to ensure proper dosage of BAPN. After euthanasia by CO_2 inhalation at 11 weeks of age, left and right femora and tibiae were removed, stripped of soft tissue, wrapped in PBS-soaked gauze and stored at −20 °C until needed.

Atomic force microscopy

From the left femur, an 8–10 mm section of the diaphysis was sectioned, mounted anterior-side up to a steel disk using cyanoacrylate glue and polished with a 3 μm diamond suspension as described previously ($n = 4$–5 per group).[22,36] Each section was treated for 14 min with 0.5 M ethylenediaminetetraacetic acid at a pH of 8.0 followed by sonication for 5 min in water, and this cycle was repeated three times. Sections were imaged using a BioScope Catalyst AFM (Bruker, Santa Barbara, CA, USA) in peak force tapping mode. 3.5 × 3.5 μm^2 images were acquired from 4 to 5 locations in each bone using a silicon nitride cantilever with a silicon probe (tip radius ∼2 nm). At each location, 10–15 fibrils were analyzed in error images (∼70 fibrils per bone) using two-dimensional fast Fourier transforms (2D FFTs) as described previously.[36–39] Briefly, 2D FFTs were performed on an area of interest over individual fibrils so that the first harmonic peak from the power spectrum represented the D-spacing for that fibril.

Nanoindentation

From the right femur, an 8–10 mm section of the diaphysis was sectioned, mounted anterior-side up to a steel disk using cyanoacrylate glue and polished with a 3 μm diamond suspension. At 3–5 locations per sample, a diamond Berkovich tip was pushed into the polished surface at 300 μN s^{-1}, held for 10 s at 3000 μN and unloaded at 300 μN s^{-1} using a 950 TI TriboIndenter (Hysitron, Minneapolis, MN, USA). Samples were kept fully hydrated in PBS during indentations. Reduced modulus (E_r) and hardness (H) were calculated using the Oliver–Pharr method.[40]

Raman spectroscopy

Left tibiae were stripped of their periosteum by scraping lightly with a scalpel. To keep the bones fully hydrated during imaging, each sample was submerged in a PBS bath with only the anterior surface exposed to air. Raman spectroscopy was performed with a LabRAM HR 800 Raman Spectrometer (Horiba Jobin Yvon, Edison, NJ, USA) with an integrated BX41 microscope (Olympus, Tokyo, Japan). Five locations were imaged ∼1 mm apart along the anterior surface of the bone, distal to the tibia–fibula junction (TFJ; $n = 4$–5 per group). A 660 nm laser was focused to a spot size of ∼10 μm using a 50 × objective (NA = 0.75) and five 20 s acquisitions were averaged at each location. After a five-point linear baseline correction in LabSpec 5 (Horiba Jobin Yvon), OriginPro 8.6 (OriginLab, Northampton, MA, USA) was used to integrate the peaks corresponding to PO_4^{3-} ν1 (∼960 cm^{-1}), CO_3^{2-} ν1 (∼1070 cm^{-1}), amide III (∼1250 cm^{-1}), CH_2 wag (∼1450 cm^{-1}) and the amide I envelope (1550–1720 cm^{-1}) as described previously.[22] Relative levels of type B carbonate substitution were found by the band area ratio of CO_3^{2-} ν1/PO_4^{3-} ν1. The band area ratios PO_4^{3-} ν1/amide I, PO_4^{3-} ν1/CH_2 wag and PO_4^{3-} ν1/amide III were calculated as metrics of matrix mineralization. In OriginPro, a single Gaussian function was fit to the PO_4^{3-} ν1 peak and the crystallinity/maturity was determined by the inverse of the full-width at half-maximum of the fitted peak.

Reference point indentation

RPI was performed using a BioDent Hfc (Active Life Scientific, Santa Barbara, CA, USA) on the anterior surface of the left tibiae using bone probe 3 while submerged in PBS ($n = 4$–5 per group). Five locations were indented ∼1 mm apart between the distal metaphysis and the TFJ, in a similar region and on the same bones as the Raman scans. Ten cycles of a 5 N indentation force were applied at a frequency of 2 Hz.

A custom Matlab (Mathworks, Natick, MA, USA) program was used to calculate the 1st cycle indentation distance (ID 1st), 1st cycle energy dissipation (ED 1st), US 1st, CID 1st, IDI, total indentation distance (TID), total energy dissipation (ED Tot), average creep indentation distance (Avg CID), average energy dissipation (Avg ED) and average unloading slope (Avg US).[41] All indentations used the same probe assembly and were performed on the same day.

Statistical analyses

For Raman, RPI and nanoindentation, multiple locations within a single sample were averaged to produce the sample value used in mean comparisons. For mean comparisons of D-spacing, fibril measurements from each sample were averaged to produce a single value of D-spacing for each sample. A two-way ANOVA was used to test the main effects of BAPN treatment, exercise and their interaction. Violations of normality or homoscedasticity were determined with a Shapiro–Wilk test or a Brown–Forsythe test, respectively ($P<0.05$). These violations were overcome with an appropriate transformation where necessary. To compare the distributions of fibril D-spacing, Kolmogorov–Smirnov tests (KS tests) were used to evaluate the effects of BAPN treatment (Sed BAPN vs Sed PBS), the effects of exercise (Ex PBS vs Sed PBS) and the ability of exercise to compensate for effects of BAPN treatment (Ex BAPN vs Sed PBS). A Bonferroni correction for multiple comparisons was used for the KS tests lowering the threshold for a comparison to be considered significant to $P<0.0167$. For all tests, SAS 9.3 (SAS Institute, Cary, NC, USA) was used for statistical comparisons. In all cases, two-sided P-values were used with $P<0.05$ considered significant. All data are presented as mean $\pm$ s.d.

Conflict of Interest

The authors declare no conflict of interest.

Acknowledgements

We thank Dr Ken Kozloff and Benjamin Sinder for training and access to the nanoindentation system. This work was supported by IUPUI departmental start-up funds, Research Support Funds Grant from the IUPUI Office of the Vice Chancellor for Research and funding from the IUPUI Biomechanics and Biomaterials Research Center.

References

1. Rho JY, Kuhn-Spearing L, Zioupos P. Mechanical properties and the hierarchical structure of bone. *Med Eng Phys* 1998;**20**:92–102.
2. Orgel JPRO, Irving TC, Miller A, Wess TJ. Microfibrillar structure of type I collagen in situ. *Proc Natl Acad Sci USA* 2006;**103**:9001–9005.
3. Traub W, Arad T, Weiner S. Three-dimensional ordered distribution of crystals in turkey tendon collagen fibers. *Proc Natl Acad Sci USA* 1989;**86**:9822–9826.
4. Gupta HS, Seto J, Wagermaier W, Zaslansky P, Boesecke P, Fratzl P. Cooperative deformation of mineral and collagen in bone at the nanoscale. *Proc Natl Acad Sci USA* 2006;**103**:17741–17746.
5. Launey ME, Buehler MJ, Ritchie RO. On the mechanistic origins of toughness in bone. *Annu Rev Mater Res* 2010;**40**:25–53.
6. Garnero P, Borel O, Gineyts E, Duboeuf F, Solberg H, Bouxsein ML *et al.* Extracellular post-translational modifications of collagen are major determinants of biomechanical properties of fetal bovine cortical bone. *Bone* 2006;**38**:300–309.
7. Yamauchi M, Sricholpech M. Lysine post-translational modifications of collagen. *Essays Biochem* 2012;**52**:113–133.
8. Haque A, Hossain M, Lambein F, Bell EA. Evidence of osteolathyrism among patients suffering from neurolathyrism in Bangladesh. *Nat Toxins* 1997;**5**:43–46.
9. Rosmus J, Trnavský K, Deyl Z. Experimental lathyrism—a molecular disease. *Biochem Pharmacol* 1966;**15**:1405–1410.
10. McKay G, Lalich J, Schilling E, Strong F. A crystalline 'Lathyrus factor' from *Lathyrus odoratus*. *Arch Biochem Biophys* 1954;**52**:313–322.
11. Siegel RC, Pinnell SR, Martin GR. Cross-linking of collagen and elastin. Properties of lysyl oxidase. *Biochemistry* 1970;**9**:4486–4492.
12. Sevil M, Anadon-Baselga M, Frejo M, Llama E, Capo M. Pharmacokinetic analysis of β-aminopropionitrile in rabbits. *Vet Res* 1996;**27**:117–123.
13. Paschalis E, Tatakis D, Robins S, Fratzl P, Manjubala I, Zoehrer R *et al.* Lathyrism-induced alterations in collagen cross-links influence the mechanical properties of bone material without affecting the mineral. *Bone* 2011;**49**:1232–1241.
14. El Rouby DH, Bashir MH, Korany NS. Ultrastructural and histomorphometric alterations of rat jaw bones after experimental induction of lathyrism. *Arch Oral Biol* 2008;**53**:916–923.
15. McNerny EMB, Gong B, Morris MD, Kohn DH. Bone fracture toughness and strength correlate with collagen cross-link maturity in a dose-controlled lathyrism mouse model. *J Bone Miner Res* 2014;**30**:455–464.
16. Saito M, Marumo K. Collagen cross-links as a determinant of bone quality: a possible explanation for bone fragility in aging, osteoporosis, and diabetes mellitus. *Osteoporos Int* 2010;**21**:195–214.
17. Warden SJ, Hurst JA, Sanders MS, Turner CH, Burr DB, Li J. Bone adaptation to a mechanical loading program significantly increases skeletal fatigue resistance. *J Bone Miner Res* 2005;**20**:809–816.
18. Wallace JM, Ron MS, Kohn DH. Short-term exercise in mice increases tibial post-yield mechanical properties while two weeks of latency following exercise increases tissue-level strength. *Calcif Tissue Int* 2009;**84**:297–304.
19. Wang X, Bank RA, TeKoppele JM, Agrawal CM. The role of collagen in determining bone mechanical properties. *J Orthop Res* 2001;**19**:1021–1026.
20. Bart ZR, Hammond MA, Wallace JM. Multi-scale analysis of bone chemistry, morphology and mechanics in the oim model of osteogenesis imperfecta. *Connect Tissue Re.* 2014;**55**(Suppl 1):4–8.
21. Gonzalez AD, Gallant MA, Burr DB, Wallace JM. Multiscale analysis of morphology and mechanics in tail tendon from the ZDSD rat model of type 2 diabetes. *J Biomech* 2014;**47**:681–686.
22. Hammond MA, Gallant MA, Burr DB, Wallace JM. Nanoscale changes in collagen are reflected in physical and mechanical properties of bone at the microscale in diabetic rats. *Bone* 2014;**60**:26–32.
23. Mantila Roosa SM, Liu Y, Turner CH. Gene expression patterns in bone following mechanical loading. *J Bone Miner Res* 2011;**26**:100–112.
24. Xing W, Baylink D, Kesavan C, Hu Y, Kapoor S, Chadwick RB *et al.* Global gene expression analysis in the bones reveals involvement of several novel genes and pathways in mediating an anabolic response of mechanical loading in mice. *J Cell Biochem* 2005;**96**:1049–1060.
25. Yerramshetty JS, Lind C, Akkus O. The compositional and physicochemical homogeneity of male femoral cortex increases after the sixth decade. *Bone* 2006;**39**:1236–1243.
26. Akkus O, Adar F, Schaffler MB. Age-related changes in physicochemical properties of mineral crystals are related to impaired mechanical function of cortical bone. *Bone* 2004;**34**:443–453.
27. McElderry J-DP, Zhu P, Mroue KH, Xu J, Pavan B, Fang M *et al.* Crystallinity and compositional changes in carbonated apatites: evidence from 31 P solid-state NMR, Raman, and AFM analysis. *J Solid State Chem* 2013;**206**:192–198.
28. Diehl KH, Hull R, Morton D, Pfister R, Rabemampianina Y, Smith D *et al.* A good practice guide to the administration of substances and removal of blood, including routes and volumes. *J Appl Toxicol* 2001;**21**:15–23.
29. Machon C, Le Calve B, Coste S, Riviere M, Payen L, Bernard D *et al.* Quantification of β-aminopropionitrile, an inhibitor of lysyl oxidase activity, in plasma and tumor of mice by liquid chromatography tandem mass spectrometry. *Biomed Chromatogr* 2014;**28**:1017–1023.
30. Trackman P, Kagan H. Nonpeptidyl amine inhibitors are substrates of lysyl oxidase. *J Biol Chem* 1979;**254**:7831–7836.
31. Nagan N, Callery PS, Kagan HM. Aminoalkylaziridines as substrates and inhibitors of lysyl oxidase: specific inactivation of the enzyme by *N*-(5-aminopentyl) aziridine. *Front Biosci* 1998;**3**:A23–A26.
32. Paschalis EP, Gamsjaeger S, Tatakis DN, Hassler N, Robins SP, Klaushofer K. Fourier transform infrared spectroscopic characterization of mineralizing type i collagen enzymatic trivalent cross-links. *Calcif Tissue Int* 2014;**96**:18–29.
33. Ricard-Blum S, Ville G. Collagen cross-linking. *Int J Biochem* 1989;**21**:1185–1189.
34. Bernard M, Yoshioka H, Rodriguez E, Van der Rest M, Kimura T, Ninomiya Y *et al.* Cloning and sequencing of pro-alpha 1 (XI) collagen cDNA demonstrates that type XI belongs to the fibrillar class of collagens and reveals that the expression of the gene is not restricted to cartilagenous tissue. *J Biol Chem* 1988;**263**:17159–17166.
35. Wallace JM, Rajachar RM, Allen MR, Bloomfield SA, Robey PG, Young MF *et al.* Exercise-induced changes in the cortical bone of growing mice are bone- and gender-specific. *Bone* 2007;**40**:1120–1127.
36. Wallace JM, Erickson B, Les CM, Orr BG, Holl MMB. Distribution of type I collagen morphologies in bone: relation to estrogen depletion. *Bone* 2010;**46**:1349–1354.
37. Fang M, Liroff KG, Turner AS, Les CM, Orr BG, Holl MMB. Estrogen depletion results in nanoscale morphology changes in dermal collagen. *J Invest Dermatol* 2012;**132**:1791–1797.
38. Wallace JM, Orr BG, Marini JC, Holl MMB. Nanoscale morphology of type I collagen is altered in the Brtl mouse model of osteogenesis imperfecta. *J Struct Biol* 2011;**173**:146–152.
39. Erickson B, Fang M, Wallace JM, Orr BG, Les CM, Banaszak Holl MM. Nanoscale structure of type I collagen fibrils: quantitative measurement of D-spacing. *Biotechnol J* 2013;**8**:117–126.
40. Oliver WC, Pharr GM. Improved technique for determining hardness and elastic modulus using load and displacement sensing indentation experiments. *J Mater Res* 1992;**7**:1564–1583.
41. Aref M, Gallant MA, Organ JM, Wallace JM, Newman CL, Burr DB *et al.* *In vivo* reference point indentation reveals positive effects of raloxifene on mechanical properties following 6 months of treatment in skeletally mature beagle dogs. *Bone* 2013;**56**:449–453.